Aerotecnica Missili & Spazio, *The Journal of Aerospace Science, Technology and Systems*

Finite elements with node dependent kinematics and scalable accuracy for the analysis of Stokes flows

D. Guarnera[a], E. Zappino[a], A. Pagani[a], E. Carrera[a]

[a] MUL^2 - Politecnico di Torino
Dipartimento di Ingegneria Meccanica e Aerospaziale

Abstract

This paper extends the use of one-dimensional elements with node-dependent kinematics to the analysis of Stokes flows. According to the Carrera Unified Formulation, the primary variables of the flow, velocity and pressure, are expressed as arbitrary expansions of the generalized unknowns. The novel implementation proposed in this work allows to increase the accuracy of the model only in the areas of the domain where it is required; i.e. close to boundaries, barriers or sudden expansion. Refined one-dimensional models based on Taylor and Lagrange expansions are used in this work and some typical applications are proposed to assess this novel technique, including Stokes flows in cylindrical and non-conventional domains. For each numerical example, different combinations of one-dimensional models have been considered to account for different kinematic approximations of flows, and the results, compared with analytical or finite volume solutions, highlight the capabilities of the proposed approach to handle non-conventional boundary conditions with ease and in preserving the computational cost without any accuracy loss.

1. Introduction

The perspective of simulating very complex fluid-dynamic systems, together with the growing necessity to decrease the computational times, influences the researchers to develop mathematical theories and numerical methods able to satisfy these requirements. The development of accurate but straightforward models does not represent an easy challenge, and often it requires the involvement of strong assumptions. Modern Computational Fluid-Dynamics (CFD), in which even a simple 3D analysis requires a considerable computational power, is well-suited to this cause, at least for flows with a prominent direction. The first reduced description of a fluid-dynamic network dates back in the 1960s and was a model with lumped parameters. In this context, the flow parameters were expressed by algebraic equations that *lump* everything in a relatively small number of parameters, similarly to electrical circuits, [1, 2]. Over time, some progress was made due to the introduction of the *transversally averaged* flows. In this case, the pressure and the flow rate are averaged in each transversal cross-section, neglecting the other components of the motion. This method allows obtaining relatively simple equations, even if it suffers the more complicated topology, [3]. Recently, these limitations have been overcome locally due to the advent of one-dimensional (1D) models for the resolution of Navier-Stokes equations. In this framework, the axial flow parameters are spread on the cross-section through different mathematical methods. Karnidakis and Sherwin [4] developed the idea of a 1D finite element model coupled to spectral/hp function; these preliminary results incouraged Pontaza and Reddy [5] to implement them with a least-square method, and Smith *et al.* to develop a finite difference scheme, [6]. More recently, an iso-geometric analysis with spectral functions has been proposed by Guzzetti *et al.* in [7].

Although the significant achievements, the problem of providing an efficient modelling methodology to describe entire networks of 1D flows (e.g., cardiocirculatory system) is still open. As an example, a detailed analysis of an artery branch cannot neglect the interaction with the rest of the cardiocirculatory system, but, at the same time, it is unthinkable to model the whole system with the same accuracy all over the problem support. Because the use of three-dimensional models for the analysis of the complete domain could lead to huge computational costs, several attempts have been done to use reduced refined models only in a small region and reduced models elsewhere. A preliminary analysis of this argument has been conducted by Formaggia *et al.* [8], whereas a multi-scale model for the coupling of one-dimensional with 2D/3D models has been proposed in Ref. [9]. The models with variable kinematics (*node-dependent kinematics*, NDK) have been proposed, for structural mechanics, by Carrera and Zappino [10], in the framework of the Carrera Unified Formulation (CUF). The node-dependent kinematic approach, as used in Ref. [11–13],

allows to change the kinematic assumptions node-by-node, as in Fig. 1. In this manner, by using the scalable properties of CUF and the finite element shape functions, the analyst can gradually increase the accuracy of the solution in determined zones of interest, without introducing any mathematical aartificies. In other words, low-order models can be combined with higher-order models with 3D accuracy without any accuracy loss if CUF-NDK methodology is used. The CUF is a one-dimensional finite elelemnt (FE) scheme capable to describe the kinematic field along the cross-section through the use of interpolation functions [14]. The 1D-CUF was initially developed for expansion functions based on Taylor series (TE) by Carrera and Giunta [15]. A new family of interpolation functions based on Lagrange polynomials has been introduced in the CUF framework by Carrera and Petrolo [16]. In this case the transversal physical domain is subdivided into a number of local expansion sub-domains, whose polynomial degree depends on the type of Lagrange expansion adopted. The 1D-CUF has been employed in many other areas of interest and refined models were used, for example for composite structures [17] and aerospace engineering [18]. As it concerns the CUF in the fluid-dynamics framework, preliminary results were discussed by Varello *et al.* in [19]. The present work aims to extend the capabilities of NDK technique to the description of incompressible and highly viscous flows. The present paper is organized as follows: (1) first, CUF-NDK technique for fluid-dynamics are presented; (2) then some numerical results are discussed and analyzed and, finally, (3) the key findings are drawn.

2. Governing equations for Fluid-Dynamics

The computational domain is assumed in a Cartesian coordinate system as depicted in Fig. 2. Ω is the domain and $\partial\Omega$ represents the boundaries, whereas Γ is referred for the orthogonal cross-sections. Let consider the Galerkin approximation of the Stokes problem for incompressible flows with homogeneous boundary condition in Eq. 1:

$$\text{Find } \mathbf{u}_h \in V_h,\ p_h \in Q_h \text{ such that}$$

$$\begin{cases} \displaystyle\int_\Omega \nu\, \nabla \mathbf{u}_h : \nabla \mathbf{v}_h \,\mathrm{d}\Omega - \int_\Omega p_h\, \nabla\cdot \mathbf{v}_h \,\mathrm{d}\Omega = \\ \qquad \displaystyle\int_\Omega \mathbf{f}\cdot \mathbf{v}_h \,\mathrm{d}\Omega & \forall\, \mathbf{v}_h \in V_h \\ \displaystyle -\int_\Omega q_h\, \nabla\cdot \mathbf{u}_h \,\mathrm{d}\Omega = 0 & \forall\, q_h \in Q_h \end{cases} \tag{1}$$

with ν as the kinematic viscosity in $[m^2/s]$ and $\mathbf{f}$ as the body forces acting in Ω. $\mathbf{u_h}$ and p_h in Eqs. 1 are the discrete solutions of velocity in $[m/s]$, and pressure in $[m^2/s^2]$, of the Stokes problem. Due to the presence of a highly viscous fluid, it is possible to neglect the non-linear term from the Navier-Stokes set of equations, referred as *linear momentum conservation* and *mass conservation*.

The terms $\mathbf{u_h}$ and p_h in Eqs. 1 are the discrete solutions of the Stokes problem in weak form. Let the bilinear forms $a : V \times V \to \mathbb{R}$ and $b : V \times Q \to \mathbb{R}$ to be defined as follows:

$$a\,(\mathbf{u},\, \mathbf{v}) \;=\; \int_\Omega \nu\, \nabla \mathbf{u} : \nabla \mathbf{v} \,\mathrm{d}\Omega \tag{2}$$

$$b\,(\mathbf{u},\, q) \;=\; -\int_\Omega q\, \nabla\cdot \mathbf{u} \,\mathrm{d}\Omega \tag{3}$$

With this notation, the Galerkin approximation of the Stokes equations reads

$$\text{Find } \mathbf{u}_h \in V_h,\ p_h \in Q_h \text{ such that}$$

$$\begin{cases} a\,(\mathbf{u}_h,\, \mathbf{v}_h) \,+\, b\,(\mathbf{v}_h,\, p_h) \;=\; (\mathbf{f},\, \mathbf{v}_h) & \forall\, \mathbf{v}_h \in V_h \\ b\,(\mathbf{u}_h,\, q_h) \;=\; 0 & \forall\, q_h \in Q_h \end{cases} \tag{4}$$

where $V_h \subset V$ and $Q_h \subset Q$ represent two families of finite dimensional subspaces depending on a real positive discretization parameter h.

2.1. One-dimensional CUF-FE models for Stokes flows

The one-dimensional Carrera Unified Formulation (CUF) is here employed to approximate the Stokes problem presented above. According to CUF, the velocity field $\mathbf{u}_h$ and the pressure field p_h are expressed, in a unified manner, as a generic expansion of the generalized unknowns through arbitrary functions of the cross-section domain coordinates:

$$\mathbf{u}_h(x,y,z) = F^U_\tau(x,z)\mathbf{u}_\tau(y), \qquad \tau = 1,2,\cdots,M^U \tag{5}$$

$$p_h(x,y,z) = F^P_m(x,z)p_m(y), \quad m = 1,2,\cdots,M^P \tag{6}$$

where $\mathbf{u}_\tau(y)$ and $p_m(y)$ are the vector of the velocity and the scalar pressure respectively, both functions of the pipe axis y. According to the CUF, F^U_τ and F^P_m correspond to the interpolation functions on the cross-section Γ, which is defined in the Cartesian plane xz, and M^U and M^P are the number of terms in the expansion, for velocity and pressure respectively. In the present work Taylor and Lagrange expansion functions are considered.

Combining the FE classic procedure with CUF (Eqs. 5, 6) the final expressions describing the unknown fields are

$$\mathbf{u}_h\,(x,\, y,\, z) \;=\; F^U_\tau\,(x,\, z)\, N^U_i\,(y)\, \mathbf{u}_{\tau i}, \qquad \tau = 1,\ldots,\, M^U \quad i = 1,\ldots,\, N^U_n \tag{7}$$

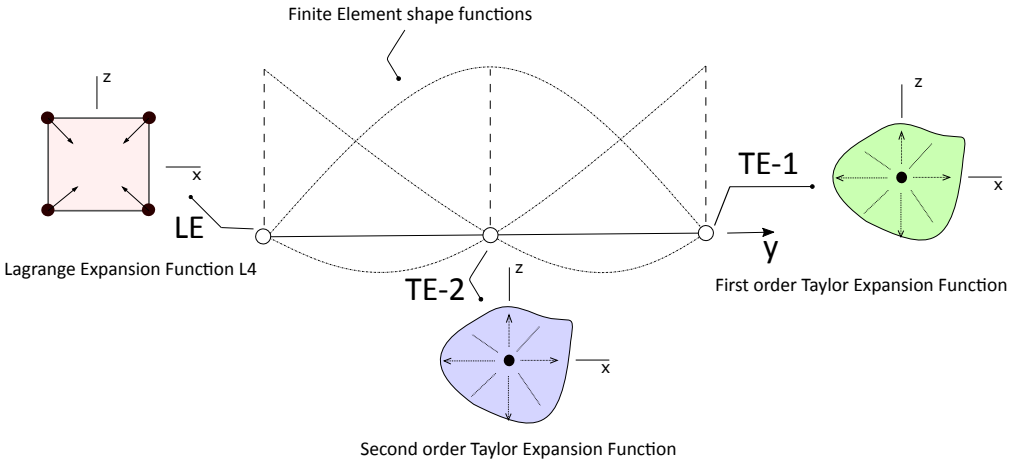

Figure 1. A three-node 1D finite element with node-dependent kinematics.

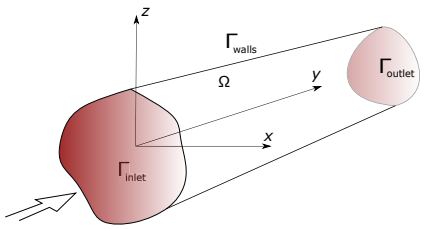

Figure 2. Computational domain Ω

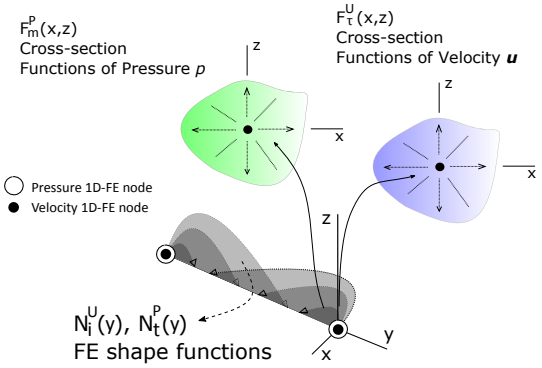

Figure 3. One-dimensional CUF-FE technique for fluid-dynamics.

$$p_h\,(x,\,y,\,z)\;=\;F_m^P\,(x,\,z)\,N_t^P\,(y)\,p_{mt},$$
$$m=1,\ldots,\,M^P\quad t=1,\ldots,\,N_n^P \tag{8}$$

where N_i^U and N_t^P are the 1D-FEM shape functions that can be arbitrary, and in general, different, and N_n^U and N_n^P represent the number of FEM nodes for velocity and pressure along the pipe axis, respectively. In this work, the classic Lagrangian 1D shape functions are considered, (see [20]). This procedure is well explained in Fig. 3, in which 1D shape functions, N_i^U and N_t^P, and cross-sectional expansions, F_τ^U and F_m^P, are represented for a schematic finite element.

2.2. CFD fundamental nuclei

According to 1D-CUF, the generic discrete test functions $\mathbf{v}_h \in V_h$ and $q_h \in Q_h$ are approximated as in Eqs. 7 and 8. It is sufficient, therefore, that the Galerkin approximation in Eq. 1 is verified for each function of the basis of V_h and Q_h, because all the functions in the spaces V_h and Q_h are a linear combination of the basis functions (see [21, 22]). Hence, the solution of the Galerkin approximation in the framework of CUF is derived by the following equations:

Find $\mathbf{u}_h \in V_h,\ p_h \in Q_h$ such that

$$\begin{cases} a\,(\mathbf{u}_h,\,\boldsymbol{\varphi}_{\tau ie})\;+\;b\,(\boldsymbol{\varphi}_{\tau ie},\,p_h)\;=\;(\mathbf{f},\,\boldsymbol{\varphi}_{\tau ie}) & \forall\tau,\ \forall i,\ \forall e \\ b\,(\mathbf{u}_h,\,\phi_{m\,t})\;=\;0 & \forall m,\ \forall t \end{cases} \tag{9}$$

with $\tau = 1,\ldots,M^U$, $i = 1,\ldots,N_n^U$, $e = 1,\ldots,3$, $m = 1,\ldots,M^P$, $t = 1,\ldots,N_n^P$. The index e refers to the three components of the velocity field, and

$$\boldsymbol{\varphi}_{\tau ie}\,(x,\,y,\,z)\;=\;\left\{\begin{array}{c}\delta_{1e}\,F_\tau^U\,(x,\,z)\,N_i^U\,(y)\\ \delta_{2e}\,F_\tau^U\,(x,\,z)\,N_i^U\,(y)\\ \delta_{3e}\,F_\tau^U\,(x,\,z)\,N_i^U\,(y)\end{array}\right\} \tag{10}$$

are the bases of the space V_h due to the 1D CUF approximation and $\delta_{\mathsf{ke}} = 1$ if $e = \mathsf{k}$, 0 otherwise. Similarly,

$$\phi_{mt}\,(x,\,y,\,z) \;=\; F_m^P\,(x,\,z)\,N_t^P\,(y) \tag{11}$$

For the sake of clarity, indices s (instead of τ) and j (instead of i) are introduced into Eq. 9 for the CUF approximation of the discrete solution $\mathbf{u}_h$ (see Eq. 7). After mathematical manipulations (see [23]), Eq. 9 becomes the following system of algebraic equations:

$$\begin{cases} \mathbf{A}^{\tau sij}\,\mathbf{q}_{sj} \;+\; \mathbf{B}^{\tau mit\,T}\,p_{mt} \;=\; \mathbf{F}^{\tau i} & \forall\,\tau,\;\; \forall\,i \\ \mathbf{B}^{mstj}\,\mathbf{q}_{sj} \;=\; \mathbf{0} & \forall\,m,\;\; \forall\,t \end{cases} \tag{12}$$

where $\mathbf{A}^{\tau sij}$ is the *fundamental nucleus* related to the bilinear form $a\,(\mathbf{u}_h,\,\boldsymbol{\varphi}_{\tau ie})$ of the 1D-CUF model;

$$\begin{aligned} \mathbf{A}^{\tau sij} \;=\; \Bigg[\; & \nu \int_L N_i^U\,N_j^U\,\mathrm{d}y \int_{\Gamma_S} F_{\tau,x}^U\,F_{s,x}^U\,\mathrm{d}\Gamma \;+ \\ & \nu \int_L N_{i,y}^U\,N_{j,y}^U\,\mathrm{d}y \int_{\Gamma_S} F_\tau^U\,F_s^U\,\mathrm{d}\Gamma \;+ \\ & \nu \int_L N_i^U\,N_j^U\,\mathrm{d}y \int_{\Gamma_S} F_{\tau,z}^U\,F_{s,z}^U\,\mathrm{d}\Gamma \Bigg]\,\mathbf{I} \end{aligned} \tag{13}$$

$\mathbf{B}^{\tau mit\,T}$ is the *fundamental nucleus* related to the bilinear form $b\,(\boldsymbol{\varphi}_{\tau ie},\,p_h)$;

$$\mathbf{B}^{\tau mit\,T} \;=\; \begin{Bmatrix} -\int_L N_i^U\,N_t^P\,\mathrm{d}y \int_{\Gamma_S} F_{\tau,x}^U\,F_m^P\;\mathrm{d}\Gamma \\ -\int_L N_{i,y}^U\,N_t^P\,\mathrm{d}y \int_{\Gamma_S} F_\tau^U\,F_m^P\;\mathrm{d}\Gamma \\ -\int_L N_i^U\,N_t^P\,\mathrm{d}y \int_{\Gamma_S} F_{\tau,z}^U\,F_m^P\;\mathrm{d}\Gamma \end{Bmatrix} \tag{14}$$

$\mathbf{B}^{mstj}$ is the *fundamental nucleus* corrisponding to the bilinear form $b\,(\mathbf{u}_h,\,\phi_{mt})$;

$$\mathbf{B}^{mstj} \;=\; \begin{Bmatrix} -\int_L N_t^P\,N_j^U\,\mathrm{d}y \int_{\Gamma_S} F_m^P\,F_{s,x}^U\,\mathrm{d}\Gamma \\ -\int_L N_t^P\,N_{j,y}^U\,\mathrm{d}y \int_{\Gamma_S} F_m^P\,F_s^U\,\mathrm{d}\Gamma \\ -\int_L N_t^P\,N_j^U\,\mathrm{d}y \int_{\Gamma_S} F_m^P\,F_{s,z}^U\,\mathrm{d}\Gamma \end{Bmatrix}^T \tag{15}$$

and $\mathbf{F}^{\tau i}$ is the *fundamental nucleus* related to the term $(\mathbf{f},\,\boldsymbol{\varphi}_{\tau ie})$.

$$\mathbf{F}^{\tau i} \;=\; \int_\Omega F_\tau^U\,N_i^U\,\mathbf{f}\,\mathrm{d}\Omega \tag{16}$$

In Eq. 13, $\mathbf{I}$ is the 3×3 identity matrix.

As in other CUF applications, the mathematical expressions of the nuclei are formally independent of the theory orders (N^U and N^P) and on the FEM shape functions (N_i^U and N_t^P). These nuclei have to be expanded against the indices τ, s, m, i, j, and t. Interested readers can find more detailes about the imposition of the boundary conditions in Ref. [23]

3. CUF for fluid-dynamics with node-dependent kinematics approach

A higher-order approximation allows to the one-dimensional models to solve complicated problems, even if the complexity is limited only to some regions of the domain. Particular inlet velocity profiles as well as pipe with non conventional geometries are examples of local problems in which is suitable a node-dependent kinematics scheme. In the CUF framework, it means to be able to adopt different interpolating functions at each node, different in terms of accuracy and family (TE/LE).

Taking into account, for instance, the fluid domain in Fig. 5, a different kinematics has been assigned at each of the FEM nodes, both for velocity and pressure. In this figure, a quadratic and a linear FE were used for the description of the velocity and pressure respectively. The expansion of the indexes in the figure depends on the kinematics assigned to each node, which determines the dimension of the elemental FE arrays associated to the Galerkin approximation of the Stokes problem in Eq. 12. In particular, the velocity field of the Fig. 5, can be written at the first node as:

$$\mathbf{u}^1 = F_\tau^1 \mathbf{u}_{1\tau}, \qquad \tau = 1, 2, \cdots, M_1^U \tag{17}$$

at the second node, the velocity field is:

$$\mathbf{u}^2 = F_\tau^2 \mathbf{u}_{2\tau}, \qquad \tau = 1, 2, \cdots, M_2^U \tag{18}$$

while at the third one is:

$$\mathbf{u}^3 = F_\tau^3 \mathbf{u}_{3\tau}, \qquad \tau = 1, 2, \cdots, M_3^U \tag{19}$$

The expansion functions F_τ^1, F_τ^2 and F_τ^3 can be chosen arbitrarily in each node. At node 1 a second-order TE model has been used, a first-order TE model has been employed at node 2 while a quadratic LE expansion has been imposed at node 3. As a result, the expression of the three-dimensional velocity field for the whole element is:

$$\begin{aligned} \mathbf{u} = F_\tau^1 N_1 \mathbf{u}_{1\tau} + F_\tau^2 N_2 \mathbf{u}_{2\tau} + F_\tau^3 N_3 \mathbf{u}_{3\tau}, \\ \tau = 1, 2, \cdots, M_i^U \end{aligned} \tag{20}$$

An analogue procedure is valid for the pressure field. The different expansions communicate one to each other through the FE shape functions N_i along the element length, in order to obtain a smooth transition of the unknown field among the three nodes. In

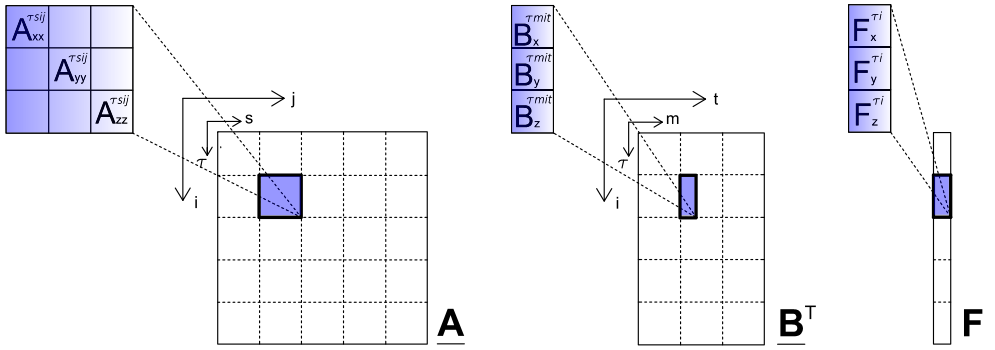

Figure 4. Procedure to build the finite element matrices and vectors expanding the fundamental nuclei. Scheme for *momentum* conservation equation.

this way, the continuity of the solution is ensured at each point. To summarize, the node-dependent feature means that:

$$F_\tau(x,z) \longrightarrow F_\tau^i(x,z) \tag{21}$$

$$M \longrightarrow M_i \tag{22}$$

where the Eq. 21 defines the expansion function as property of the nodes and not of the element, and the number of terms in the expansion, M, can be different at each node, as in Eq. 22 and the i underlines this aspect. Finally, the general equations of the variable fields are:

$$\begin{aligned} \mathbf{u} &= F_\tau^i N_i \mathbf{u}_{i\tau}, \\ &\tau = 1,2,\cdots,M_i^U; i = 1,\cdots,N_n^U \end{aligned} \tag{23}$$

$$\begin{aligned} p &= F_m^t N_t p_{tm}, \\ &m = 1,2,\cdots,M_t^P; t = 1,\cdots,N_n^P. \end{aligned} \tag{24}$$

This feature allows to control the dimension of the matrices to save computational costs. For further detailes about the CUF-NDK, see Ref. [10,24,25], where this methodology has been employed for the analysis of elastic structures.

4. Numerical Results

The section hereinafter shows the efficiency of the method explained above, through some numerical examples. The refined models proposed are compared with the analytical solution whenever possible, or with solutions obtained by finite volumes tools. The first example aims to assess the NDK approach in the case of the Poiseuille flow in a cylindrical pipe. The present models have been than used to study flows with different inlet velocities distributions whereas the last example tests the node-dependent kinematics formulation in the case of square-section pipes.

All the examples consider a pipe with a length L of $6m$, a radius $r = 1m$ and, in case of square section, a side of $s = 2m$; the pipe always presents a homogeneous Dirichlet boundary condition at lateral walls and a homogeneous Neumann boundary condition at the outlet section. The inlet section presents some non-homogeneous Dirichlet boundary conditions, that have been specified for each case. No body forces are applied and the fluid has a viscosity, ν, equal to $10^{-2}m^2/s$ to satisfy the condition of $RE \ll 1$. All the cases hold a discretization of ten one-dimensional elements along the main axis, B3 for pressure and B4 for velocity. All the one-dimensional models considered hereinafter are implemented and solved in FORTRAN environment. For the sake of clarity, the following nomenclature has been used to denote models with different kinematic assumptions:

- nLE^{t^U,t^P}: Model with uniform Lagrange Expansion; n is the number of elements used for the cross-section description and t is the type of elements used for velocity and pressure, i.e. four-nodes LE4 or nine-nodes LE9 elements.
- TE^{N^U,N^P}: Taylor models with order N^U and N^P for the velocity and pressure fields respectively.
- $TE/LE/TE$: NDK scheme with Taylor and Lagrange Expansions.

As an example, with $TE^{4,2}$ it is denoted a Taylor

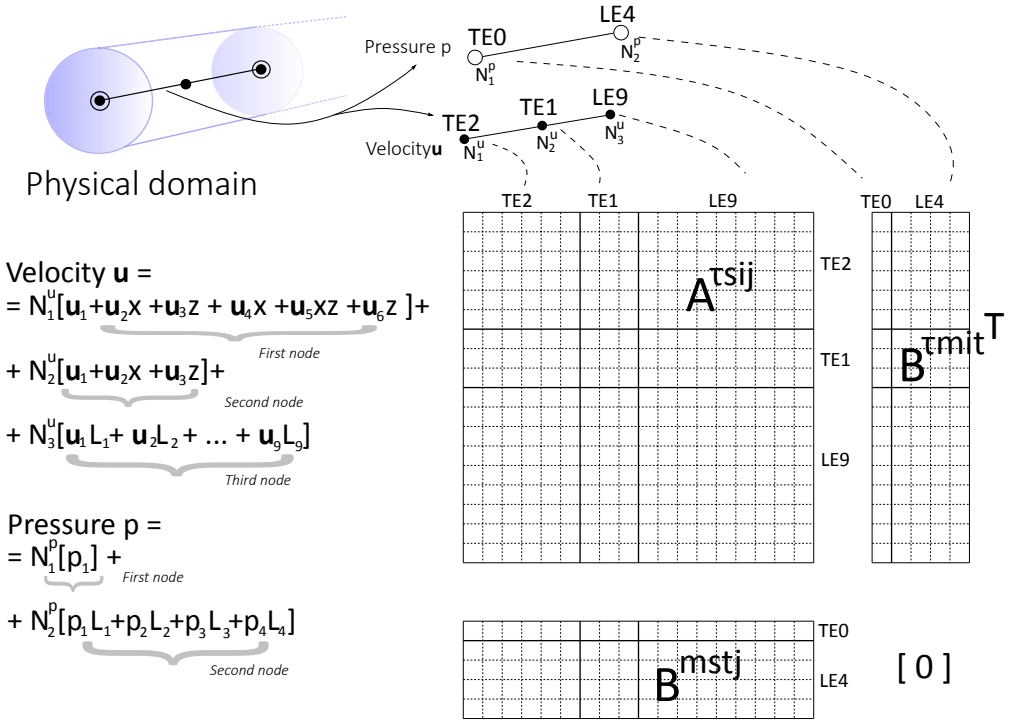

Figure 5. FEM model of fluid-dynamics model using node-dependent kinematics. The expansion of the velocity and of the pressure fields change node-by-node and this determines the dimension of the matrices.

model with a fourth order expansion for the velocity field and a second order expansion for the pressure distribution. On the other hand, with $4LE^{9,4}/TE^{3,1}$ is denoted a model with a LE kinematics in a part of the domain, and a $TE^{3,1}$ models elsewhere.

4.1. Poiseuille flow analysis

The first numerical assessment takes into account the Poiseuille flow in a cylinder. Since the analytical solution is available, this simple application has been used to assess the NDK approach proposed in the present paper. In particular the results obtained with the node-dependet kienmatic one-dimensional models have been compared with those obtained with constant kienmatic models and the analysical solution, [19, 26]. A parabolic distribution of velocity was enforced at the inlet, with $u_y = 10^{-4}$ m/s at the center of the section. Figure 6 shows the pressure distribution along the axial direction obtained with the different 1D models, while in Fig. 7 it is possible to see the comparison between the 1D node-dependent kinematics model and the Poiseuille analytical solution regarding the axial velocity. The results clearly show that, even if the kinematic is modified along the duct, the 1D models describe very well the Poiseuille flow. In particular, as the Fig. 7 suggests, the models can describe the parabolic distribution of the u_y across the section and are able to keep it on constant along the whole pipe, in accordance with the analytical solution.

4.2. Analysis of flow with different inlet velocity profiles

The Poiseulle flow has been used to assess the one -dimensional node-dependent kinematics models. The natural decreasing of the pressure, as well as the parabolic distribution of the velocity, was not affected by the change of the kinematics along the duct. In this section, the advantages of the NDK method have been exploited to investigate flow with complex velocity profiles at the inlet cross-section.

The first example considered is a flow in a cylindrical pipe with a fourth-order Dirichlet boundary condition at the inlet. Equation 25 shows the three components of the velocity imposed at the inlet section, where u_y is the component parallel to the pipe axis.

$$\begin{cases} u_x = 0 \\ u_y = 10^{-4}\left(1 - x^2 - z^2\right)^2 \\ u_z = 0 \end{cases} \qquad \text{on } \Gamma_D^{\text{in}} \qquad (25)$$

As seen in Ref. [19], it is necessary at least a $TE^{4,2}$ model to detect the distribution of the velocity across the inlet section. Since the flow tends to become parabolic moving away from the inlet section, it could

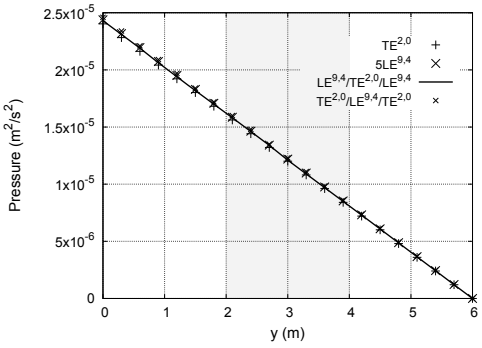

Figure 6. Pressure trends of the Poiseuille flow. Comparison between constant and node-dependent kinematic one-diemnsional models. The grey part defines the region of domain in which NDK models change the kinematics.

Table 1
Values of pressure at inlet and midspan sections. Comparison of CUF-1D results. Fourth-order inlet velocity profile.

Model	$p(m^2/s^2)$ - Inlet	$p(m^2/s^2)$ - Midspan
$TE^{4,2}$	$1.79e-5$	$8.0080e-6$
$TE^{4,2}$ / $TE^{2,0}$	$1.78e-5$	$8.0079e-6$
$TE^{2,0}$	-510536	70.4931

be possible to decrease the expansion orders, as in Fig. 8, saving computational effort. Differently from the Poiseuille flow case, the pressure has not a complete linear decrease along the duct, that is the $N^P = 0$ is not sufficient in the area closest the inlet cross-section, as is evident in Table 1. Neverthless, the possibility to have more refined kinematic in the inlet area, allows to describe the pressure trend correctly as evident in Fig. 9, decreasing the computational effort as well. Figure 10 shows how the distribution of the axial velocity changes along the duct. In particular, the velocity moves from a 4^{th}-order curve to a 2^{nd}-order one (Poiseuille-like), and, due to this, it is not necessary to keep the expansion order $N^U = 4$ for the entire pipe. It is possible to decrease the expansion order from 4 to 2, without any loss of accuracy, as evident in Fig. 10 where one-dimensional constant and node-dependent kinematic models are compared with OpenFOAM solutions. The primary advantage of the method here presented is in terms of computational costs, as shown in Table 2. In this table, the maximum values of pressure at the inlet and the maximum values of velocity at the midspan cross-section evaluated using different models are enlisted. As in

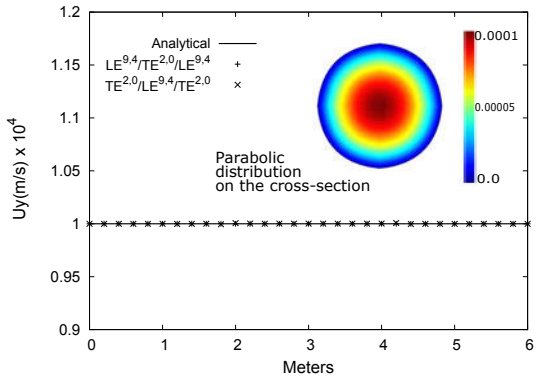

Figure 7. Velocity trends of the Poiseuille flow. Comparison between constant and node-dependent kinematic one-diemnsional models.

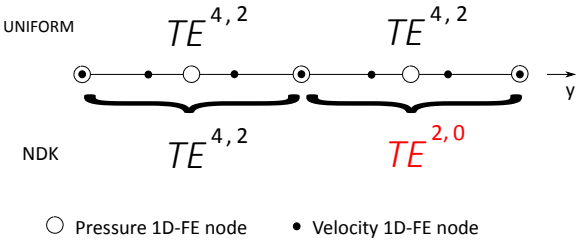

Figure 8. Node-dependent kinematics scheme of fourth-order inlet velocity case. Changing of expansion order for velocity N^U and pressure N^P node-by-node.

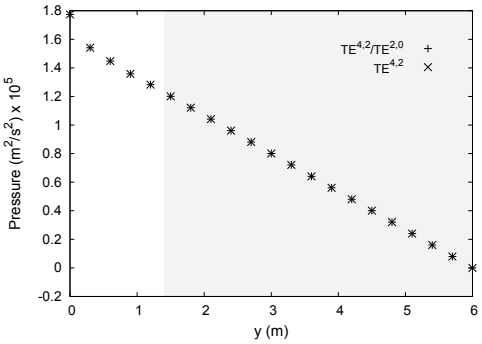

Figure 9. Comparison of the pressure path between uniform and NDK 1D-CUF models. The grey area denotes the domain where the $TE^{2,0}$ model has been used. Fourth-order inlet velocity profile.

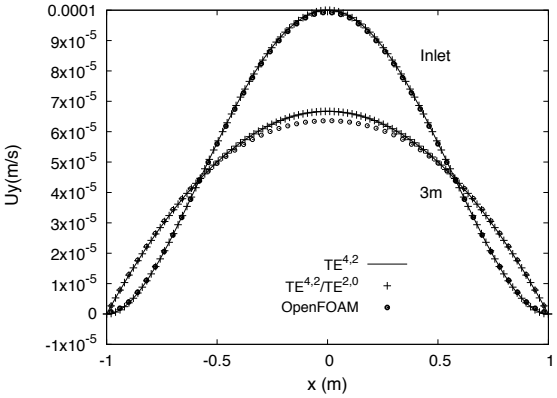

Figure 10. Comparison of the velocity distribution between 1D-CUF models and OpenFOAM results at inlet and midspan cross-section. Fourth-order inlet velocity profile.

Table 2
Maximum value of pressure at inlet y=0m and maximum axial velocity at midspan y=3m. Comparison among different 1D-CUF results and OpenFOAM solutions . Fourth-order inlet velocity profile.

Model	$p \times 10^5 (m^2/s^2)$	$u_y \times 10^5 (m/s)$	$DOFs$
	OpenFOAM		
$OpenFOAM_a$	1.70	6.50	10560
$OpenFOAM_b$	1.79	6.53	54400
	TE		
$TE^{4,3}$	1.79	6.66	2031
$TE^{4,2}$	1.79	6.66	2031
	LE		
$5LE^{9,4}$	1.75	6.53	2493
$5LE^{16,9}$	1.82	6.67	5361
	NDK		
$TE^{4,2}$ / $TE^{2,0}$	1.78	6.66	852

Table 3
Maximum value of pressure at inlet y=0m and maximum axial velocity at midspan y=3m. Comparison among different 1D-CUF results and OpenFOAM solutions. Fifth-order inlet velocity profile.

Model	$p \times 10^6 (m^2/s^2)$	$u_y \times 10^5 (m/s)$	$NDOF$
	OpenFOAM		
$OpenFOAM_a$	8.17	2.44	54400
$OpenFOAM_b$	9.08	2.35	435520
	TE		
$TE^{6,5}$	9.23	2.50	4095
$TE^{6,4}$	10.72	2.50	3909
$TE^{5,4}$	10.80	2.50	3048
	LE		
$9LE^{16,9}$	9.19	2.50	9045
$20LE^{16,9}$	9.36	2.50	19818
	NDK		
$TE^{6,5}$ / $TE^{2,0}$	9.09	2.50	1379

Ref. [19], the reference solution was obtained using the CFD code OpenFOAM [27]. As the Table 2 suggests, the possibility to reduce the expansion order node-by-node does not affect the accuracy of the solution and allows a reduction of DOFs.

A non-simemtric Dirichlet boundary condition has been considered as second case. A fifth-order distribution of velocity is enforced at the inlet cross-section, according to the Eq. 26.

$$\begin{cases} u_x = 0 \\ u_y = 10^{-4}\left(1 - x^2 - z^2\right)\left(1/4 + xz + x^3\right) & \text{on } \Gamma_D^{\text{in}} \\ u_z = 0 \end{cases} \tag{26}$$

The meshes along the y-axis remain unvaried, as well as the other boundary conditions. Since the inlet flow is no more axisymmetric, as shown in Fig. 11, the one-dimensional models need high-order expansions to describe the profiles of both velocity ($N^U = 6$) and pressure ($N^P = 5$), ([19]). Since the boundary conditions lead the flow to become Poiseuille-like, it can be convenient to predict the model by using a node-dependent kinematic approach. The variation of the velocity profile is visible in Fig. 12, in which 1D models, with constant and node-dependent kinematic, are compared to the OpenFOAM solutions. The goodness of the results obtained is confirmed also numerically by the Table 3, in which the values of pressure at the inlet and velocity at the midspan are compared among different models. At the end of these analyses, it is possible to make the following comments:

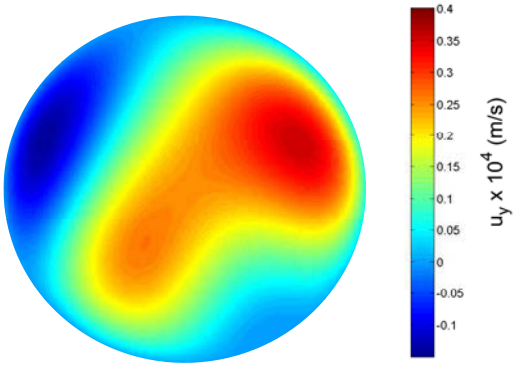

(a) Velocity distribution

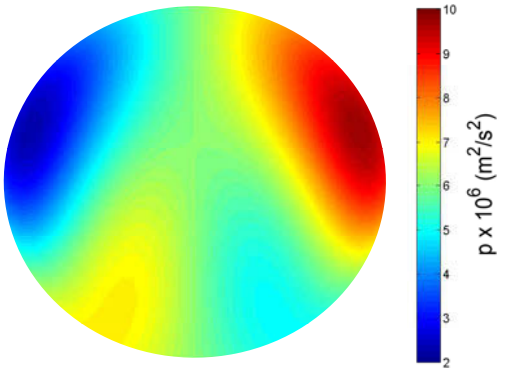

(b) Pressure distribution

Figure 11. Fifth-order inlet boundary condition, distributions across the section. Velocity (a) and pressure (b).

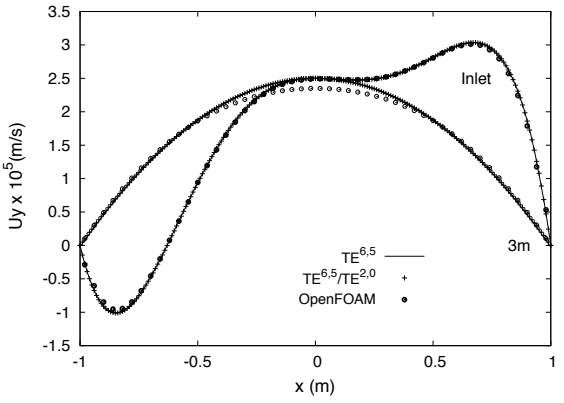

Figure 12. Comparison of the velocity distribution between 1D-CUF models and OpenFOAM results at inlet and midspan cross-section. Fifth-order inlet velocity profile.

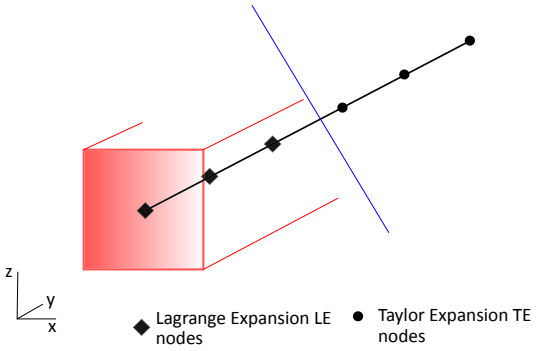

Figure 13. Scheme of the one-dimensional model with mixed kinematics LE/TE.

- One-dimensional models are able to predict the evolution of complex flows in presence of different Dirichlet boundary conditions at the inlet.

- The models with node-dependent kinematics allow to describe flow parameters without any loss of accuracy and saving computational effort when compared to commercial tool solutions.

4.3. Analysis of a flow in a square-section pipe

The validation of one-dimensional models with node-dependent kinematics has been conducted through the example of the Poiseuille flow in a circular cylinder and then has been confirmed by applying the method to more complex flows. The last numerical example is related to a second-order flow in a square-section pipe. In this case, the aim is to demonstrate the capability of the present method also in the analysis of non-conventional pipes and to show the capabilities of a model with a mixed LE/TE kinematics, as shown in the scheme in Fig. 13. The flow considered keeps the same viscosity of the previous cases as well as for the boundary conditions on the outlet and lateral surfaces. At the inlet section, a second-order velocity profile is enforced. Figure 14 shows the behavior of the pressure field along the square-section pipe. TE models have not a good response at the beginning of the pipe, even using higher-order polynomials. This approach leads to an accurate descritpion of the velocity and the pressure fields, even in the proximity of the inlet cross section where a $4LE^{9,4}$ model is used. At the same time, the use of a $TE^{4,0}$ models elsewhere entails a reduction of the computational costs. The kinematics changing at the 8^{th} node does not affect the model: the flow, in fact, keeps on his parabolic nature, as in Fig. 15.

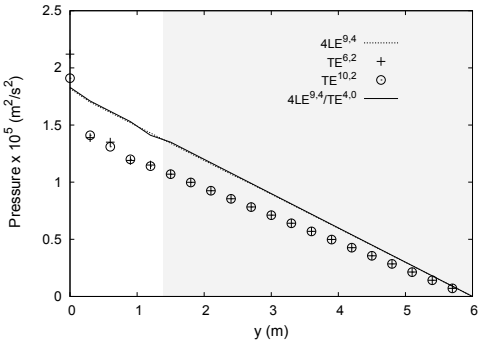

Figure 14. Comaprison of pressure trends for different one-dimensional models. The grey area denotes the domain where the NDK model with $TE^{4,0}$ model has been used.

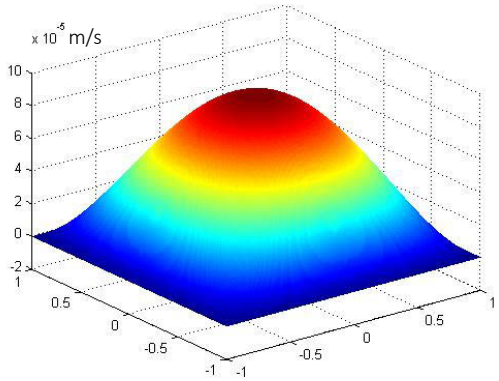

Figure 15. Parabolic shape of axial velocity at 8^{th} where the kinematics changes.

5. Conclusions

In this work, the Carrera Unified Formulation has been used for the description of incompressible, laminar and viscous flows in pipes. In particular, the novel node-dependent kinematics technique has been extended to the analysis of axial flows. According to the CUF, the flow parameters are expressed as expansion of the generalised unknowns and this is possible through some interpolation functions, that can be different on each node. Different numerical examples have been considered to demonstrate the effectiveness of the present approach. Different 1D models have been employed to describe Poiseuille and higher-order flows in circular and square-section pipes. The results obtained by one-dimensional NDK models have been compared with the analyitical solution or with finite volume solutions coming from OpenFOAM freeware tool. The following considerations can be drawn from the results:

- Both 1D models, with uniform or node-dependent kinematics, are able to provide accurate results in comparison with the analytical solution.
- The NDK models provide results with a high grade of accuracy and allow a substantial saving of computational effort, with respect to the 3D solution.
- The NDK appraoch does not introduce any inconsistency in the kinematic transition area, that is, the continuity of the velocity and pressure field is respected.

The outcomes of this research demostrates how the one-dimensional reduced models can be accurate and convenient: the efficiency of NDK models should be considered as the starting point on the modelization of complex networks as the cardiocirculatory system.

Conflict of interest

On behalf of all authors, the corresponding author states that there is no conflict of interest.

REFERENCES

1. V. C. Rideout and D. E. Dick. Difference-differential equations for fluid flow in distensible tubes. *IEEE Transactions on Biomedical Engineering*, 14(3):171–177, 1967.
2. N. Westerhof, F. Bosman, C.J. De Vries, and A. Noordergraaf. Analog studies of the human systemic arterial tree. *Journal of Biomechanics*, 2(2):121–143, 1969.
3. J. Ottesen. A fluid dynamical model of the aorta with bifurcations. *Tekst 297, Rotskilde Univ.*, 1995.

4. G. Karniadakis and S. Sherwin. *Spectral/Hp Element Methods for CFD (Numerical Mathematics and Scientific Computation)*. Oxford University Press, New York, 1999.
5. J.P. Pontaza and J.N. Reddy. Spectral/hp least-squares finite element formulation for the Navier-Stokes equations. *Journal of Computational Physics*, 190(2):523–549, 2003.
6. N.P. Smith, A.J. Pullan, and P.J. Hunter. An anatomically based model of transient coronary blood flow in the heart. *SIAM Journal of Applied Mathematics*, 62(3):990–1018, 2002.
7. S. Guzzetti, S. Perotto, and A. Veneziani. Hierarchical model reduction for incompressible fluids in pipes. *International Journal for Numerical Methods in Engineering*, 114(5):469–500, 2017.
8. L. Formaggia, F. Nobile, A. Quarteroni, and A. Veneziani. Multiscale modelling of the circulatory system: a preliminary analysis. *Computing and visualization in science*, 2(2-3):75–83, 1999.
9. L. Formaggia, J.F. Gerbeau, F. Nobile, and A. Quarteroni. On the coupling of 3D and 1D Navier - Stokes equations for flow problems in compliant vessels. *Computational Methods in Applied Mechanics and Engineering*, 191(6-7):561–582, 2001.
10. E. Carrera and E. Zappino. One-dimensional finite element formulation with node-dependent kinematics. *Computers & Structures*, 192:114–125, 2017.
11. E. Carrera, E Zappino, and G Li. Finite element models with node-dependent kinematics for the analysis of composite beam structures. *Composites Part B: Engineering*, 132:35–48, 2018.
12. E. Carrera, M. Filippi, and E. Zappino. Node-dependent kinematic one-dimensional models for the analysis of rotating structures. In *ASME 2017 International Mechanical Engineering Congress and Exposition*, Tampa, Florida, US, November 2017. American Society of Mechanical Engineers.
13. G. Zappino, E.and Li and E. Carrera. Node-dependent kinematic elements for the dynamic analysis of beams with piezo-patches. *Journal of Intelligent Material Systems and Structures*, 29(16):3333–3345, 2018.
14. E. Carrera, M. Cinefra, M. Petrolo, and E. Zappino. *Finite element analysis of structures through Unified Formulation*. Wiley, 2014.
15. E. Carrera and G. Giunta. Refined beam theories based on a unified formulation. *International Journal of Applied Mechanics*, 2(1):117–143, 2010.
16. E. Carrera and M. Petrolo. Refined beam elements with only displacement variables and plate/shell capabilities. *Meccanica*, 47(3):537–556, 2012.
17. G. Giunta, F. Biscani, S. Belouettar, A.J.M. Ferreira, and E. Carrera. Free vibration analysis of composite beams via refined theories. *Composites Part B: Engineering*, 44(1):540 – 552, 2013.
18. E. Carrera, M. Petrolo, and A. Varello. Advanced beam formulations for free-vibration analysis of conventional and joined wings. *Journal of Aerospace Engineering*, 25(2):282–293, 2012.
19. A. Varello, A. Pagani, D. Guarnera, and E. Carrera. Analysis of Stokes flows by Carrera Unified Formulation. *Advances in Aircraft and Spacecraft Science*, 5(3):363–383, 2018.
20. O.C. Zienkiewicz, R.L. Taylor, and R.L. Taylor. *The finite element method*, volume 3. McGraw-hill London, 1977.
21. A. Quarteroni. *Numerical Models for Differential Problems*, volume 1. Springer, 2009.
22. F. Brezzi. On the existence, uniqueness and approximation of saddle-point problems arising from Lagrange multipliers. *Revue Francaise de Automatique, Informatique, Recherche Operationnelle. Analyse Numerique*, 8:129–151, 1974.
23. A. Varello. Advanced higher-order one-dimensional models for fluid-structure interaction analysis. *Ph.D Thesis - Politecnico di Torino*, 2013.
24. E. Zappino, G. Li, A. Pagani, and E. Carrera. Global-local analysis of laminated plates by node-dependent kinematic finite elements with variable esl/lw capabilities. *Composite Structures*, 172:1–14, 2017.
25. E. Carrera, E. Zappino, and G. Li. Finite element models with node-dependent kinematics for the analysis of composite beam structures. *Composites Part B: Engineering,*, 132:35–48, 2018.
26. S. Stera and R. Skalak. *The history of Poiseuille's Law*. 1993.
27. OpenFOAM Fundation. OpenFOAM. www.openfoam.com, 2011–2014.